Optical Engineering

SPIEDigitalLibrary.org/oe

Short-wave infrared, medium-wave infrared, and long-wave infrared imaging study for optical readout microcantilever array infrared sensing system

Cheng Gong
Yuejin Zhao
Liquan Dong
Mei Hui
Xiaomei Yu
Xiaohua Liu

SPIE

Short-wave infrared, medium-wave infrared, and long-wave infrared imaging study for optical readout microcantilever array infrared sensing system

Cheng Gong
Yuejin Zhao
Liquan Dong
Mei Hui
Beijing Institute of Technology
Key Laboratory of Biomimetic Robots and Systems
Ministry of Education, School of Optoelectronics
Beijing 100081, China
E-mail: yjzhao@bit.edu.cn

Xiaomei Yu
Peking University
Institute of Microelectronics
National Key Laboratory of Nano/Micro Fabrication Technology
Beijing 100871, China

Xiaohua Liu
Beijing Institute of Technology
Key Laboratory of Biomimetic Robots and Systems
Ministry of Education, School of Optoelectronics
Beijing 100081, China

Abstract. We aim to study the short-wave infrared (SWIR), medium-wave infrared (MWIR), and long-wave infrared (LWIR) imaging ability based on optical readout bimaterial microcantilever focal plane array (FPA) uncooled infrared imaging system. First, the principle of the bimaterial microcantilever sensing and the fabrication of the microcantilever array are introduced. Second, the optical-thermal-mechanical sensing theories based on the FPA are given. Finally, an optical readout microcantilever FPA infrared imaging system is developed for SWIR, MWIR, and LWIR imaging experiments. The experimental results show that the system can acquire the clear images of the SWIR, MWIR, and LWIR targets. © *The Authors. Published by SPIE under a Creative Commons Attribution 3.0 Unported License. Distribution or reproduction of this work in whole or in part requires full attribution of the original publication, including its DOI.* [DOI: 10.1117/1.OE.52.2.026403]

Subject terms: bimaterial microcantilever; optical readout; short-wave infrared imaging; medium-wave infrared imaging; long-wave infrared imaging.

Paper 121269 received Sep. 5, 2012; revised manuscript received Jan. 3, 2013; accepted for publication Jan. 16, 2013; published online Feb. 5, 2013.

1 Introduction

Multiband infrared (IR) imaging technology is a hotspot in the IR imaging field. It has been widely used in scientific research, medical diagnostics, energy exploration, environmental monitoring and other fields, by which the target's multiband radiation information can be acquired and the dynamic range of infrared imaging is extended effectively. In recent years, much attention has been focused on uncooled IR imaging using an optical readout bimaterial microcantilever array. In this promising technological platform, infrared radiation detection is based on the thermal mechanical deflection of individual microcantilevers owing to the absorption of infrared photons. Compared with the thermoelectric-typed uncooled IR imaging system, it eliminates the need for the highly complex and sensitive readout integrated circuits and scanning electronics, thus reducing fabrication complexity and costs.[1] The technology has been developed by a number of groups and the researches highlighted in Refs. 2 through 12 have demonstrated varying degrees of success. In 2006, our team started on uncooled microcantilever array IR imaging research. In 2008, a high sensitivity microcantilever focal plane array was designed and manufactured.[13] In 2012, Gong et al. proposed an optical readout method based on a narrow-strip filter for microcantilever array imaging[14] and analyzed the tolerable target temperature for the optical readout focal plane array (FPA) IR imaging.[15]

Previous studies have shown that the bimaterial microcantilever array can respond to dual-band medium-wave/long-wave infrared radiation[9] and terahertz (THz) radiation.[10] However, few studies have focused on imaging for the short-wave infrared (SWIR), medium-wave infrared (MWIR), and long-wave infrared (LWIR). In this paper, we aim to study these three wavebands infrared imaging ability based on the optical readout bimaterial microcantilever FPA uncooled infrared imaging system. Above all, we introduced the bimaterial microcantilever IR sensing principle and the fabrication of the microcantilever FPA. Then, the optical-thermal-mechanical sensing theory based on the FPA was given. Next, an optical readout microcantilever IR imaging system with the special designed SWIR, MWIR, LWIR through-window and lens was developed for demonstration. Meanwhile, the SWIR, MWIR, and LWIR targets were selected according to their radiation characteristics for the IR imaging experiments. The experimental results show that the bimaterial microcantilever FPA responds well to the three wavebands of infrared radiation. The theories and results are presented.

2 Principle and Theory

2.1 *Principle of the Bimaterial Microcantilever FPA*

Figure 1(a) shows the structure of a bimaterial microcantilever FPA pixel; Fig. 1(b) is an FPA photo captured by a scanning electron microscope. As shown in Fig. 1(a), the pixel structure consists of an absorber/reflector, two bimaterial deflection arms, and two thermal isolation arms. The absorber/reflector of a microcantilever pixel has

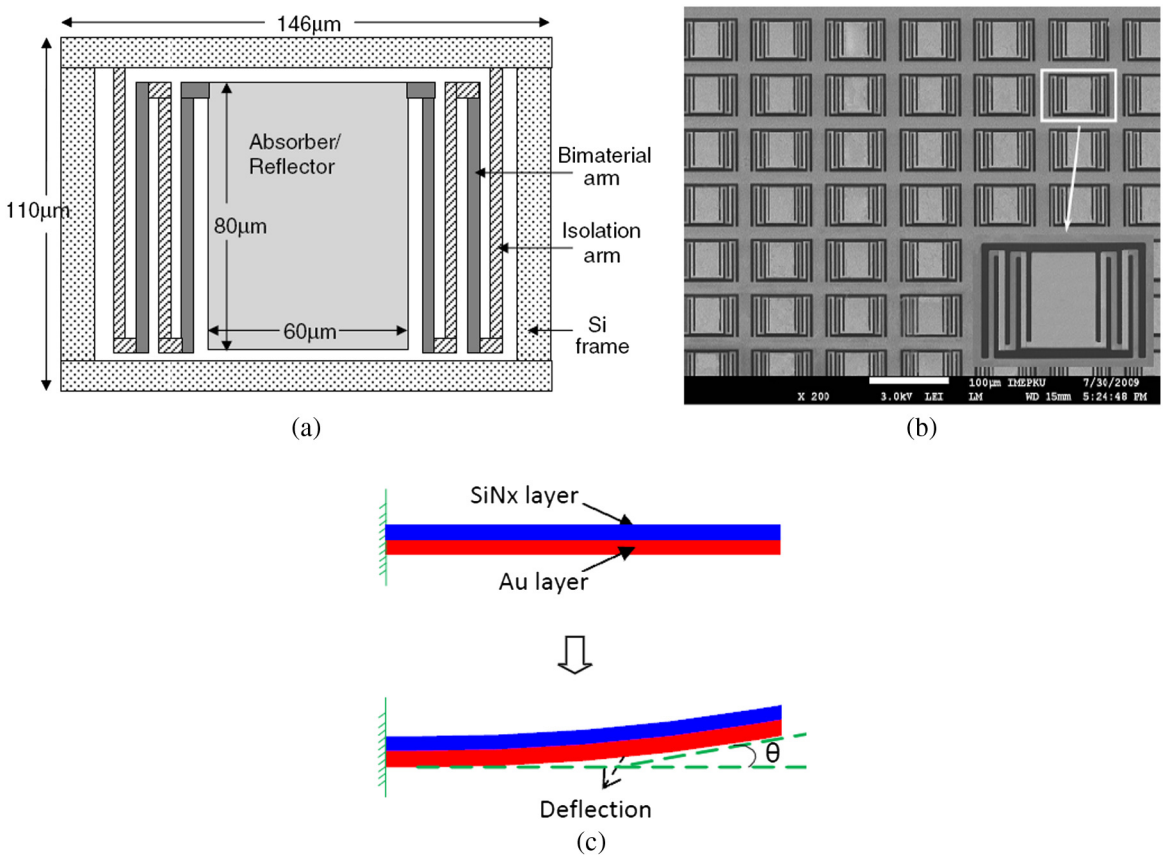

Fig. 1 (a) Structure of a microcantilever FPA pixel, (b) an FPA photo captured by a scanning electron microscope, and (c) deflection of the bimaterial cantilever under IR radiation.

one layer made of an IR absorber made by SiNx and the other layer as a visible light reflector made by Au. Figure 1(c) shows deflection of the bimaterial microcantilever under IR radiation. When IR radiation is incident on the FPA, the absorber converts the radiation to heat and transfers the heat to the connected bimaterial deflection arms. The arms are made of two kinds of materials: SiNx and Au. Since these two materials have different thermal expansion coefficients, the cantilevers bend with the change of temperature and drive the connected reflectors to change their deflection angles. The target infrared radiation can then be detected by reading out the deflection angles. The isolation arms are a layer of SiNx, whose extremely low thermal conductance thermally isolates the pixels from the supporting substrate.

2.2 *Fabrication of the Bimaterial Microcantilever FPA*

A bulk silicon micromachining process, which is schematically shown in Fig. 2, has been developed to fabricate the bimaterial microcantilever FPA. The fabrication starts with a double side polished silicon wafer with a thickness of 300 μm. The detailed micromachining steps are introduced as follows: first, an SiO_2 film of 200 nm is deposited to form the etching buffer layer between the structure layer and the substrate, and a layer of low stress SiNx of 1 μm is deposited with the low pressure chemical vapor deposition method.

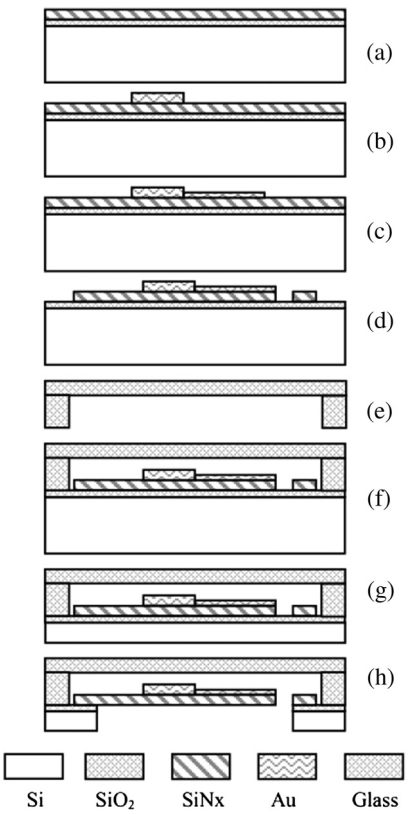

Fig. 2 Fabrication process of the FPA.

Second, a 500 nm Au film is sputtered and patterned to form the bimaterial arms with a wet etching technique. Third, in order to decrease the bending and the surface roughness of the cantilever reflector, only 50 nm Au film is sputtered and patterned as the reflecting mirror on the SiNx absorber with a lift off technique. Next, the SiNx cantilever structure is patterned and etched with reactive ion etching (RIE) technique. Fifth, a glass wafer is patterned and etched to form a 60 μm deep cavity with the cavity dimension the same as the FPA. Then the glass and silicon wafers are anodic bonded together. Here, the glass wafer is used as a supporting wafer to avoid the thin FPA structure to be broken. Next, the silicon wafer is thinned down to 100 μm in KOH solution to increase etching uniformity and decrease footing effect in the following inductively coupled plasmas (ICP) etching. In the penultimate stage, double-side lithography is used to pattern the backside silicon. At last, the silicon substrate is anisotropically etched in ICP system and the SiO_2 buffer layer is etched in RIE system to release the cantilevers.

In this process, silicon-glass anodic bonding and deep reactive ion etching (DRIE) techniques are introduced to selectively remove the substrate silicon at the area where the cantilevers are located and form a silicon frame for each of the cantilever pixels. Figure 1(b) shows an FPA photo captured by a scanning electron microscope.

2.3 *Optical-Thermal Transducing Theory of SWIR, MWIR, and LWIR*

We define the wavelength range of SWIR from 1 to 3 μm, the range of MWIR from 3 to 8 μm, and the range of LWIR as 8 to 14 μm. It is known that the temperature of bimaterial microcantilever will change owing to the absorption of infrared radiation. The optical-thermal transducing calculation theory based on different wavebands can be given by the following two steps. The first step is to calculate the change of energy to temperature per unit area in the SWIR, MWIR, and LWIR wavebands respectively. The second is to get the microcantilever's temperature change caused by the IR target's temperature change according to the first step's results.

Above all, $(dP/dT)_{\lambda 1-\lambda 2}$ is defined as the change of energy to temperature per unit area in the specific IR waveband. The calculation formula of dP/dT can be expressed as[16]

$$\frac{dP}{dT}=\frac{c_1c_2e^{c_2/\lambda T}}{\lambda^6T^2(e^{c_2/\lambda T}-1)^2}\cong\frac{c_1}{\lambda^5(e^{c_2/\lambda T}-1)}\times\frac{c_2}{\lambda T^2}, \tag{1}$$

where $e^{c_2/\lambda T}\gg 1$. Here c_1 stands for the first radiation constant and c_2 is the second radiation constant, λ is the wavelength of IR radiation. Then $(dP/dT)_{\lambda 1-\lambda 2}$ is given by

$$(dP/dT)_{\lambda 1-\lambda 2}=v_{\lambda 1-\lambda 2}\times\int_{\lambda 1}^{\lambda 2}\left(\frac{dP}{dT}\right)\mathrm{d}\lambda. \tag{2}$$

Here $v_{\lambda 1-\lambda 2}$ represents the infrared radiation conversion efficiency (absorptivity) of the bimaterial microcantilever pixel, $\lambda 1-\lambda 2$ stands for the specific IR waveband, $\lambda 1$ is the minimum wavelength and $\lambda 2$ is the maximum wavelength. The different values of v in different IR wavebands can be gotten by the measurement results of Nicolet Magna 750 Fourier Transform Infrared Spectrometer. The values of v are about 35%, 38%, and 61% in the SWIR, MWIR, and LWIR wavebands.

Next, the cantilever temperature change caused by the temperature change of the IR target source can be expressed as[17]

$$\Delta T=\frac{A\varepsilon\tau\pi(dP/dT)_{\lambda 1-\lambda 2}}{4F_{\mathrm{no}}^2(G_{\mathrm{arm}}+G_{\mathrm{rad}})}\times\Delta T_s, \tag{3}$$

where A stands for the cantilever pixel's absorption area, τ is the transmission efficiency of the infrared through-window, ε is the emissivity of the pixel, F_{no} is the ratio of aperture and focal length of the infrared lens ($F_{\mathrm{no}}=1$), G_{arm} is the thermal conductance of the thermal isolation arm, and G_{rad} is the radiation conductance of the FPA pixel. The radiation conductance G_{rad} of the microcantilever pixel can be expressed as

$$G_{\mathrm{red}}=4A_{\mathrm{pixel}}(\varepsilon_{\mathrm{Au}}+\varepsilon_{\mathrm{SiN}})\sigma T_b^3. \tag{4}$$

Here, A_{pixel} represents the total area of a microcantilever cell, ε is the emission efficiency ($\varepsilon_{\mathrm{SiNx}}=0.8$, $\varepsilon_{\mathrm{Au}}=0.01$), σ is Stefan-Boltzmann constant ($\sigma=5.67\times 10^{-8}\ \mathrm{W\cdot m^{-2}\cdot K^4}$), T_b stands for the room temperature (300 K). As is shown in Fig. 1(a), A_{pixel} is $146\times 110\ \mu\mathrm{m}^2$ in this paper. The leg's conductance G_{arm} can be calculated using

$$G_{\mathrm{arm}}=A_{\mathrm{arm}}k_{\mathrm{SiN}}/L_{\mathrm{arms}}, \tag{5}$$

where A_{arm} stands for the cross-section area of the thermal isolation arm, k_{SiN} is the thermal conductivity of the material, and L_{arms} is the total length of the thermal isolation arms. For this paper, the thickness of the arm is 0.75 μm, the width of the arm is 3 μm, the total length of the isolation is $4\times 80\ \mu$m, and the conductance of SiNx is $5.5\ \mathrm{W\cdot m^{-1}\cdot K^{-1}}$.

2.4 *Thermal-Mechanical Response Theory of the Bimaterial Microcantilever*

It is known that the bimaterial microcantilever will deflect an angle with the change of its temperature and the thermal-mechanical response theory is the same in different IR wavebands. The following two steps can be used to express the thermal-mechanical response calculation method: (1) get the microcantilever deflection δ according to its temperature change ΔT; (2) calculate the deflection angle θ corresponding to the deflection δ.

The bimaterial microcantilever deflection δ cased by the temperature change ΔT in a microcantilever can be expressed as[5]

$$\delta=3(\alpha_{\mathrm{Au}}-\alpha_{\mathrm{SiN}})\left(\frac{n+1}{K}\right)\left(\frac{L_m^2}{d_{SiN}}\right)\times\Delta T. \tag{6}$$

Here, $n=d_{\mathrm{Au}}/d_{\mathrm{SiN}}$, $K=4+6n+4n^2+\phi n^3+(\phi n)^{-1}$, $\phi=E_{\mathrm{Au}}/E_{\mathrm{SiN}}$, d is the thickness of the film ($d_{\mathrm{SiN}}=750$ nm, $d_{\mathrm{Au}}=500$ nm), α stands for the coefficient of thermal expansion ($\alpha_{\mathrm{SiN}}\alpha_{\mathrm{SiN}}=0.8\times 10^{-6}\ \mathrm{K^{-1}}$, $\alpha_{\mathrm{Au}}=14.2\times 10^{-6}\ \mathrm{K^{-1}}$), L_m is the length of the bimaterial arm ($L_m=80\ \mu$m) and E represents the elastic modulus ($E_{\mathrm{SiN}}=180$ GN/m, $E_{\mathrm{Au}}=73$ GN/m).

Then, the microcantilever deflection δ can be expressed as $\delta = L_{\text{arm}} \times \sin(\theta)$ where L_{arm} is the length of the bimaterial arm ($L_{\text{arm}} = 80\ \mu\text{m}$), so the deflection angle θ can be obtained by $\theta = \arcsin(\delta / L_{\text{arm}})$.

3 Experiments

3.1 *Prototype of the Microcantilever IR Imaging System*

An optical readout bimaterial microcantilever FPA uncooled IR imaging system was developed for the SWIR, MWIR, and LWIR imaging experiments. Figure 3 shows the schematic of the system. The FPA is placed in a vacuum chamber with a coating IR through-window for passing specified waveband of infrared radiation (three types of IR through-window and lens were used for passing the SWIR, MWIR, and LWIR radiation respectively). The specified IR lens, which can pass the specified wavebands of IR radiation and focus the target's temperature distribution on the FPA, is placed between the target and the vacuum chamber. Visible light from a green light emitting diode (LED) is collimated to parallel light and reflected by a reflector, then reflected by a beam splitter, and then irradiates the FPA. Lens 1 and lens 2 form an optical 4f system. A spatial filter (narrow-strip filter) is placed on the spectrum plane. The spectra of the FPA have a portion of their intensity curtained off under the action of it. A charge-coupled device (CCD) is placed on the image plane to acquire IR image. A more detailed description of the system based on a narrow-strip filter optical readout approach can be found in Ref. 14.

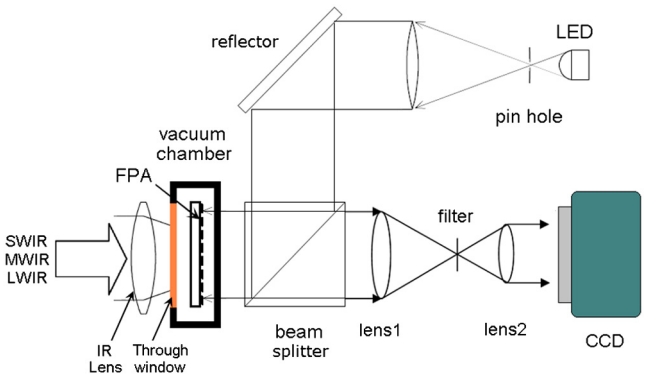

Fig. 3 Schematic of the microcantilever FPA uncooled IR imaging system.

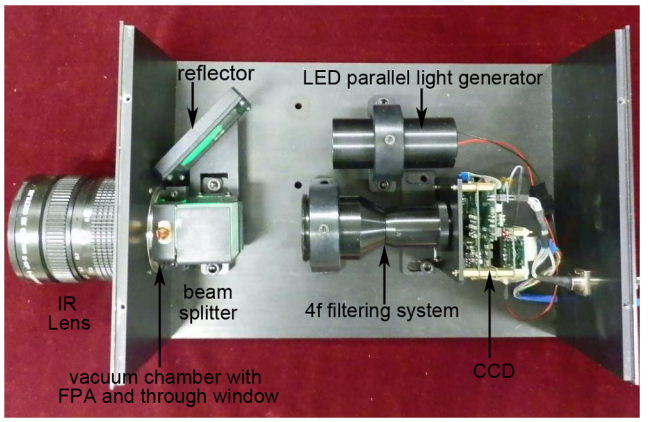

Fig. 4 Setup of the microcantilever FPA IR imaging system.

Figure 4 is a top-view photograph of the integrated experimental setup. As shown in Fig. 4, the part that produces the LED collimated light beam has been integrated as an LED parallel light generator. Lens 1, lens 2, and the spatial filter have been integrated as a 4f filtering system; the IR through-window and lens can be replaced in different wavebands IR imaging experiments. In addition, the atmospheric pressure in the vacuum chamber is 1 Pa; the number of FPA pixels is 160×120; the CCD is a 14-bits CCD, and its signal-to-noise ratio is 56 dB.

3.2 *Imaging Experiments for SWIR, MWIR, and LWIR*

The SWIR, MWIR, and LWIR imaging experiments were conducted by changing the different wavebands of IR through-window and lens. In the short-wave infrared imaging experiment, the SWIR through-window is made of quartz and the SWIR target is an SWIR laser (the SWIR lens is not necessary because the laser beam has been focused). In the medium-wave infrared imaging experiment, the through-window and infrared lens are made of germanium glass. The glass is coated for passing medium-wave infrared radiation. The selected MWIR target is a 673.15 K electric iron. According to the Planck formula, we can draw the curve of the target object radiation. Planck formula is as follows:

$$M = \frac{c_1}{\lambda^5} \frac{1}{e^{c_2/kT} - 1}, \tag{7}$$

where M represents the radiant exitance, T is the target object's temperature, λ represents the radiation wavelength, and k stands for the Boltzmann constant ($k = 1.380662 \times 10^{-23}\ \text{J}^{-2} \cdot \text{K}^4$). It is known that the first radiation constant is $c_1 = 3.741832 \times 10^{-16}\ \text{W} \cdot \text{m}^2$, the second radiation constant is $c_2 = 1.438786 \times 10^{-2}\ \text{m} \cdot \text{K}$, and the temperature $T = 673.15$ K. Accordingly, we can draw the radiant exitance curve using λ as the abscissa and M as the vertical axis. Figure 5(a) shows the radiant exitance curve of the electric iron and it can be seen that the radiation range of the electric iron belongs to the medium-wave infrared band mainly.

It is known that the center wavelength of the SWIR laser beam is 1.319 μm. In theory, the absolute temperature of the blackbody can be calculated by Wien's displacement law $\lambda_{\max} = b/T$, where $\lambda_{\max}$ is the peak wavelength, T is the absolute temperature of the black body, and b is a constant of proportionality called Wien's displacement constant, equal to $2.8977685 \times 10^{-3}\ \text{m} \cdot \text{K}$. So, according to Wien's displacement law, the absolute temperature of the blackbody corresponding to the peak wavelength 1.319 μm is about 2197 K. Figure 5(b) shows the radiant exitance curve of 2197 K target, and we can see that the absolute temperature corresponding to the peak wavelength 1.319 μm is about 2197 K.

In the long-wave infrared imaging experiment, the through-window and infrared lens are also made of germanium glass, but different from the MWIR experiment, the glass is coated for passing through LWIR infrared radiation. The selected LWIR target is a person's head. It is well known that the human body temperature is about 310.15 K.

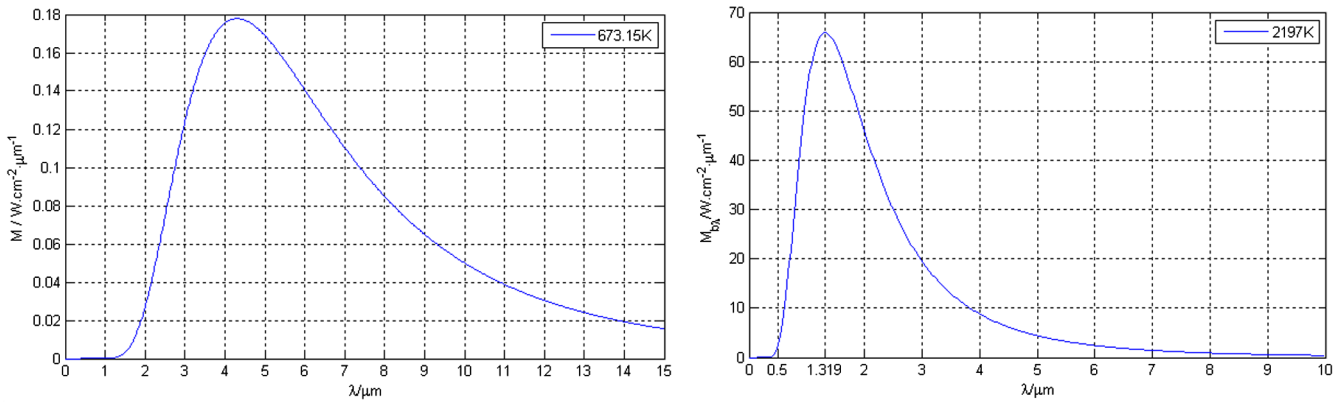

Fig. 5 (a) Radiant exitance curve of MWIR target object (673.15 K electric iron); (b) Radiant exitance curve of 2197 K target (SWIR laser).

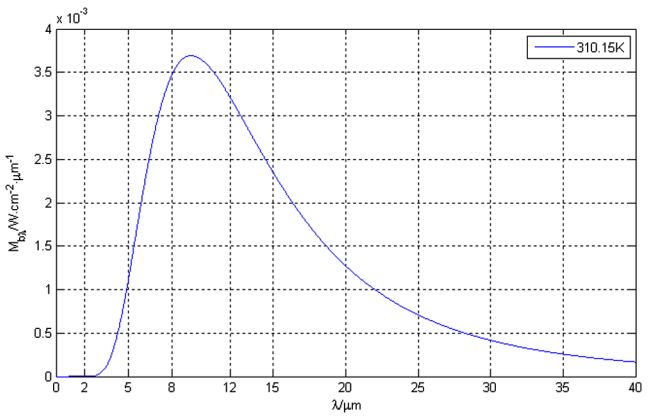

Fig. 6 Radiant exitance curve of LWIR target object (a person's head).

Therefore, its radiant exitance curve can be drawn by Planck formula. As shown in Fig. 6, it can be seen that the selected target radiates LWIR infrared mainly.

Next, the SWIR, MWIR, and LWIR imaging experimental results based on the optical readout bimaterial microcantilever uncooled IR imaging system are given. Figure 7(a) is the infrared image of SWIR target (SWIR laser beam); Fig. 7(b) shows the imaging result of MWIR target (673.15 K electric iron); Fig. 7(c) is the infrared image of LWIR target (a person's head) captured by the system. As shown in Fig. 7, the clear infrared images of the SWIR, MWIR, and LWIR targets have been obtained successfully. The results prove that the microcantilever FPA responds well to SWIR, MWIR, and LWIR radiation.

4 Conclusions

In summary, this paper focused on the SWIR, MWIR, and LWIR imaging ability of the bimaterial microcantilever array infrared imaging system. First, the principle of the bimaterial microcantilever infrared sensing and the fabrication of the microcantilever array were introduced. Second, the optical-thermal transducing calculation theory and the thermal-mechanical response calculation method based on the FPA were given. Third, an optical readout bimaterial microcantilever IR imaging system with the special designed SWIR, MWIR, LWIR through-window and lens was developed. Meanwhile, the SWIR, MWIR, and LWIR targets were selected for the three wavebands infrared imaging experiments. The experimental results show that the bimaterial microcantilever IR imaging system can obtain the clear images of the SWIR, MWIR, and LWIR targets. It provides us with a reliable experimental basis to design an optical readout microcantilever multiband IR imaging system.

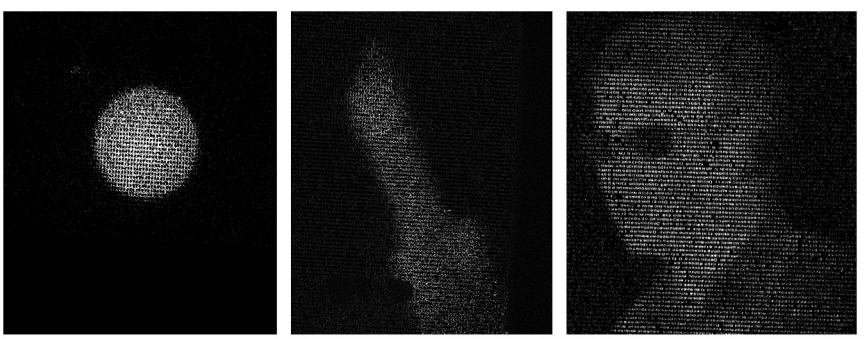

Fig. 7 (a) The infrared image of SWIR target, (b) the infrared image of MWIR target, and (c) the infrared image of LWIR targets.

Acknowledgments

This work was supported by the State Key Program of National Natural Science Foundation of China (No. 61036006), the National Natural Science Foundation of China (No. 61177094).

References

1. A. Rogalski, "Infrared detectors: status and trends," *J. Progress Quant. Electron.* **27**(2–3), 59–210 (2003).
2. S. R. Manalis et al., "Two-dimensional micro-mechanical bimorph arrays for detection of thermal radiation," *J. Appl. Phys. Lett.* **70**(24), 3311–3313 (1997).
3. K. T. Perazzo et al., "Infrared vision using uncooled micro-optomechanical camera," *J. Appl. Phys. Lett.* **74**(23), 3567–3569 (1999).
4. T. Ishizuya et al., "Optically readable bi-material infrared detector," *Proc. SPIE* **4369**, 342–349 (2001).
5. Y. Zhao et al., "Optomechanical uncooled infrared imaging system: design, microfabrication, and performance," *J. Microelectromech. Syst.* **11**(2), 136–145 (2002).
6. D. Grbovic et al., "Uncooled infrared imaging using bimaterial microcantilever arrays," *J. Appl. Phys. Lett.* **89**(7), 073118 (2006).
7. F. Dong et al., "An uncooled optically readable infrared imaging detector," *Sens. Actuat. A-Phys.* **133**(1), 236–242 (2007).
8. J. P. Salerno, "High frame rate imaging using uncooled optical readout photomechanical IR sensor," *Proc. SPIE* **6542**, 65421D (2007).
9. M. Erdtmann, L. Zhang, and G. Jin, "Uncooled dual-band MWIR/LWIR optical readout imager," *Proc. SPIE* **6940**, 694012 (2008).
10. D. Grbovic et al., "Arrays of SiO_2 substrate-free micromechanical uncooled infrared and terahertz detectors," *J. Appl. Phys.* **104**(5), 054508 (2008).
11. Q. Hao, Q. Zhu, and Y. Hu, "Random phase-shifting interferometry without accurately controlling or calibrating the phase shifts," *Opt. Lett.* **34**(8), 1288–1290 (2009).
12. C. D. W. Jones et al., "MEMS thermal imager with optical readout," *Sens. Actuat. A-Phys.* **155**(1), 47–57 (2009).
13. X. Yu et al., "Design and fabrication of a high sensitivity focal plane array for uncooled IR imaging," *J. Micromech. Microeng.* **18**(5), 057001 (2008).
14. C. Gong et al., "An optical readout method based on narrow-strip filter for microcantilever array sensing," *Opt. Lett.* **37**(7), 1187–1189 (2012).
15. C. Gong et al., "The tolerable target temperature for bimaterial microcantilever array infrared imaging," *Opt. Laser Technol.* **45**, 545–550 (2013).
16. J. M. Lloyd, *Thermal Imaging Systems*, Plenum Press, New York (1975).
17. P. W. Kruse, "Principle of uncooled infrared focal plane arrays," *Semicond. Semimet.* **47**, 17–44 (1997).

Cheng Gong received his BS degree from the School of Information Science and Technology, Beijing Institute of Technology in 2006 and his MS degree in 2009. He is currently a PhD student at the School of Optoelectronics, Beijing Institute of Technology. His current research interests include a wide variety of topics in the area of MEMS-based focal plane array infrared/terahertz imaging technology, digital image processing, and information optics.

Yuejin Zhao is a professor of Beijing Institute of Technology, School of Optoelectronics. He received his PhD degree in optical engineering, Beijing Institute of Technology in June 1990. Currently, he is a disciplinary responsibility to the team leader of "Instrument Science and Technology," in Beijing Institute of Technology. He has been engaged in teaching and research work in the field of optoelectronic instruments. His current research interests include terahertz imaging technology based on MEMS-infrared imaging technology, space optical technology, and intelligent photoelectric instrument development. He is the deputy director of the Standing Committee of Optical Society of China, vice chairman of China Instrument Society of Optical and Electrical Machinery and Systems Integration Technology branch.

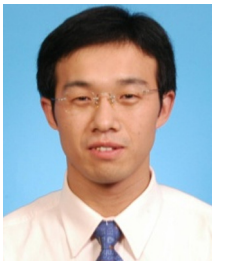

Liquan Dong graduated from the Department of Optical Engineering of Beijing Institute of Technology in 2000 with a BS degree in optical instrumentation. From then on, he joined the Night View and Infrared Technology Laboratory with focus on the infrared focal plane array nonuniformity correction. He obtained a PhD degree in optical engineering from the Beijing Institute of Technology in March 2007. He is currently an associate professor in the School of Optoelectronics and holds a joint appointment with the electro-optics program. He is a member of SPIE, OSA, COS, and CIS, and the president of SPIE Beijing Institute of Technology Chapter. His research interests include a wide variety of topics in the area of infrared focal plane array, digital signal and image processing, with emphasis on signal and image restoration.

Mei Hui received her PhD degrees from Xi'an Institute of Optics and Precision Mechanics of Chinese Academy of Science in 2001. She is currently an associate professor in the School of Optoelectronics, Beijing Institute of Technology. His current research interests include phase-shifting interferometry, segmented mirror co-phasing testing, infrared MEMS system imaging and mechanical design.

Xiaomei Yu received her PhD degrees in material engineering from Beijing University of Aeronautics and Astronautics in 2001. She is currently a professor in the Institute of Microelectronics, Peking University. At Peking University, she has carried out research in cantilever-based biochemical sensors, integrated analysis systems, silicon-based 3-D nano-fabrication technologies. Currently, her research interests are in MEMS-based IR and broadband terahertz detection, which focus on the design, fabrication, and packaging of bimaterial cantilever FPA.

Xiaohua Liu is an associate professor with the Advanced Photoelectric Instrument Laboratory in Beijing Institute of Technology. He received his BS degree from the Department of Physics, Peking University in 1983 and his MS degree from the Department of Optical Engineering, Beijing Institute of Technology in 1988. His current research interests include the terahertz technology, infrared imaging, and advanced imaging systems.